ACS APPLIED MATERIALS & INTERFACES

Research Article

Cite This: ACS Appl. Mater. Interfaces 2019, 11, 35247−35254

www.acsami.org

Controlled Spacing between Nanopatterned Regions in Block Copolymer Films Obtained by Utilizing Substrate Topography for Local Film Thickness Differentiation

Elisheva Michman,[†] Marcel Langenberg,[‡] Roland Stenger,[‡] Meirav Oded,[†] Mark Schvartzman,[§] Marcus Müller,*[,‡] and Roy Shenhar*[,†]

[†]The Institute of Chemistry and the Center for Nanoscience and Nanotechnology, The Hebrew University of Jerusalem, Jerusalem 9190401, Israel

[‡]Institute for Theoretical Physics, Georg-August-University Göttingen, Friedrich-Hund-Platz 1, 37077 Göttingen, Germany

[§]Department of Materials Engineering and Ilse Katz Institute for Nanoscale Science and Technology, Ben Gurion University of the Negev, Beer Sheva 8410501, Israel

Supporting Information

ABSTRACT: Various types of devices require hierarchically nanopatterned substrates, where the spacing between patterned domains is controlled. Ultraconfined films exhibit extreme morphological sensitivity to slight variations in film thickness when the substrate is highly selective toward one of the blocks. Here, it is shown that using the substrate's topography as a thickness differentiating tool enables the creation of domains with different surface patterns in a fully controlled fashion from a single, unblended block copolymer. This approach is applicable to block copolymers of different compositions and to different topographical patterns and thus opens numerous possibilities for the hierarchical construction of multifunctional devices.

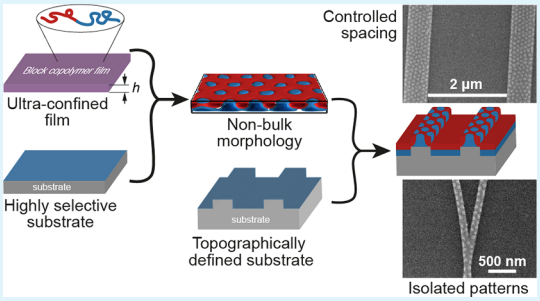

KEYWORDS: *block copolymer, directed self-assembly, thin film*

INTRODUCTION

The ability to create regions of a desired pattern on a surface and arbitrarily space between them with nonpatterned regions is a prerequisite in various applications, including metasurfaces,[1,2] bit-patterned media,[3] hybrid integrated circuits that involve plasmonic components,[4] regulating cell functions,[5−7] and sensing.[8] For example, controlling the distances between elements of a metasurface enables tuning of its optical response,[9] and the spacing between plasmon waveguides is necessary for avoiding cross-talk between adjacent channels through which signals are routed.[10]

Considerable recent progress in the directed self-assembly of block copolymers (BCPs) now enables not only fabricating thin films with highly aligned domains[11−18] but also obtaining complex morphologies such as various meshes,[19−22] layered structures,[23−26] nonregular patterns,[27−35] and mixed morphologies.[36−42] These dense structures are obtained through the application of elegantly designed processes that combine nanofabrication and self-assembly steps. The most important directed self-assembly approaches rely on either chemoepitaxy,[11,12] that is, the orientation and registration of copolymer domains that are directed by a chemically patterned, two-dimensional substrate, or graphoepitaxial alignment using a topographically patterned substrate.[15−18,43−45] Graphoepitaxy has the advantage of being three-dimensional (3D) in nature, which could be used to induce truly three-dimensionally structured BCP films (e.g., meshes).[19−21]

Despite the considerable progress in directed self-assembly, obtaining patterned regions with defined shapes that are separated by nonpatterned domains remains a challenge. One option is to utilize chemical patterning to locally control the domain orientation, but it requires multiple fabrication steps and fine-tuning of BCP/homopolymer blend compositions.[30] Subtractive approaches like imprinting into BCP films,[46,47] local etching,[48] and relying on dewetting[18,49−53] leave exposed substrates, undesired residual material, and more complex interfaces, which may not be compatible with further fabrication steps. Here, we show that topographical features could be used to modulate local film thicknesses, which, under specific circumstances, leads to the formation of dual morphologies in a controlled fashion. Taking advantage of the fact that lying lamellae show no surface pattern enables arbitrary separation between patterned domains.

Received: July 21, 2019
Accepted: September 4, 2019
Published: September 4, 2019

DOI: 10.1021/acsami.9b12817
ACS Appl. Mater. Interfaces 2019, 11, 35247−35254

RESULTS AND DISCUSSION

Samples featuring 100 μm-long stripes etched into silicon substrates (i.e., trenches) were prepared using standard electron-beam lithography followed by reactive ion etching (see the Supporting Information for additional details). Each sample included the same array of patterns differing in widths of the trenches (in the range of 160−2000 nm) and plateaus (in the range of 160−640 nm). Sets of samples featuring trench depths of 8, 13, and 20 nm were spin-coated with BCP solutions, yielding films with thicknesses in the range of 21−24 nm, which are all higher than the trench depth. All films were annealed under chloroform vapor for 15 min. Chloroform was selected for solvent annealing because it is rather nonselective toward polystyrene (PS) and poly(methyl methacrylate) (PMMA) ($\chi_{CHCl_3,\ PS}$ and $\chi_{CHCl_3,\ PMMA}$ values calculated using Hansen solubility parameters equal 0.47 and 0.50, respectively).[54]

Figure 1 shows the scanning electron microscopy (SEM) and scanning force microscopy (SFM) images of 23 nm-thick polystyrene-*block*-poly(methyl methacrylate) (PS-*b*-PMMA) films (f_{PS} = 0.48) cast on topographically defined substrates. The block copolymer organizes in the bulk into alternating lamellae with 84 nm periodicity. Interestingly, the film displays two types of morphology. The featureless appearance of the film in the trenches suggests the formation of lamellae oriented parallel to the trench floor. However, the film on the plateaus displays a dot pattern despite the near symmetric composition of the copolymer. This dual pattern is insensitive to the lateral width of the trenches (which spans 160−2000 nm in this study; see additional images in the Supporting Information, Figure S1), pointing to the ability to obtain dot-patterned regions that are arbitrarily separated by featureless domains.

The formation of a dot pattern from a lamellar BCP is attributed to the combination of strong thickness confinement and high substrate selectivity.[55] Simulations of a soft, highly coarse-grained model of symmetric BCP on flat substrates are presented in Figure 2a,b for various film thicknesses, h, and substrate selectivity values, ΛN. The systems were quenched from a disordered melt to incompatibility χN = 30 (see the Supporting Information for additional details). As expected, the top panels show that selective substrates give rise to lying lamellae, where the copolymer chains are oriented normal to the substrate on average. Upon decreasing the film thickness, we observe a transition from lying lamellae oriented parallel to the substrate to standing, perpendicularly oriented lamellae (Figure 2a, bottom row), where the copolymer chains lie flat on the substrate. The reason for this transition is that it reduces the amount of the PS/PMMA interfaces per chain.[56,57] SFM images of BCP films cast at different thicknesses on flat substrates corroborate these results (Figure S2).

In a window of film thicknesses near $0.5R_e$ and a surface preference near ΛN = 11, the symmetric diblock copolymer gives rise to a dot pattern at the surface, which corroborates the experimental observation. Interestingly, however, the three-dimensional structure that gives rise to this pattern is not the classical cylindrical morphology, but rather a complex, neck-like hexagonal morphology (Figure 2a, middle row; see cross section in Figure 2b). This unconventional morphology for a film thickness significantly less than $0.5L_0$ can be rationalized by the combination of extreme frustration of the lying morphology and a relatively strongly preferential substrate.[55,58,59] In this morphology, the bottom half of the film

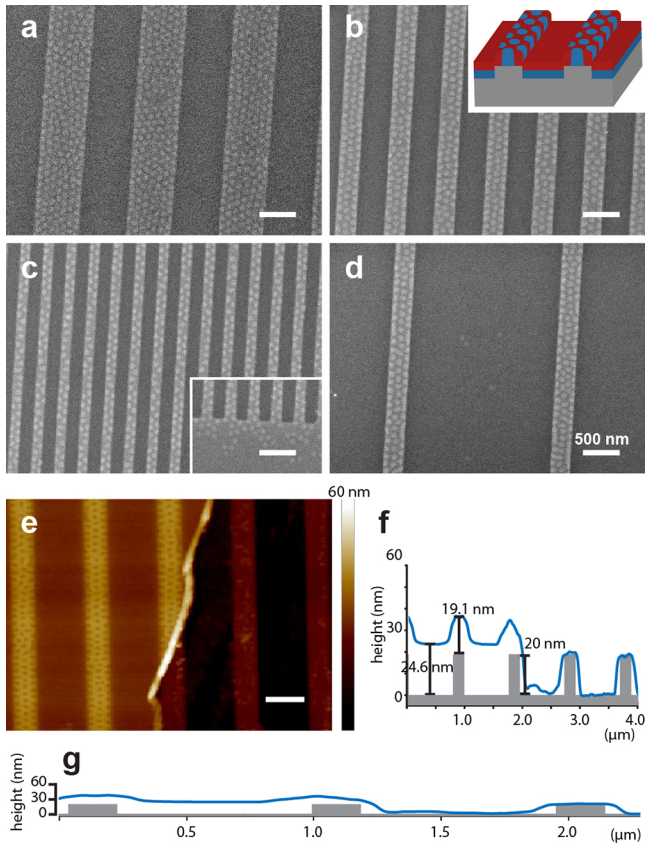

Figure 1. PS-*b*-PMMA films showing dot-patterned regions spaced arbitrarily by patternless domains assembled on topographically modified substrates. (a−d) SEM images of 23 nm-thick films assembled on substrates featuring (a) 13 nm deep and (b−d) 20 nm deep trenches. Trench/plateau lateral widths: (a) 640/640, (b) 360/320, (c) 160/160, and (d) 2000/320 nm. Inset in (b) shows a schematic illustration of a simplistic three-dimensional morphology based on the classical diblock copolymer phases; inset in (c) shows the edge of the lithographically patterned area. (e) SFM height image and (f, g) height profile of an area that was partially exposed by scratching (nominal film thickness, 23 nm; trench depth, 20 nm; trench/plateau widths, 640/320 nm). The height profile is overlaid on a schematic illustrating the substrate topography. (g) Same profile as in (f) with a 2:1 height/width ratio. All scale bars represent 500 nm.

is enriched in PMMA that preferentially wets the substrate, whereas the top half of the film is depleted in PMMA, forming a hexagonal pattern. The morphology consists of neck-like PMMA domains, similar to the cone morphology that has been previously proposed by Han et al.[60] We note here that the formation of islands and holes, which is common for film thicknesses that are incommensurate with the wetting conditions, is less favorable in the case of ultrathin films because hole formation requires exposing the high surface energy substrate (i.e., dewetting).

The combination of thickness confinement and strong substrate selectivity leads to extreme sensitivity of the morphology to the local film thickness. Hence, the formation of different morphologies on the plateaus and in the trenches suggests that the thicknesses of the BCP film above each region are different.[61,62] Partially exposing the substrate by scratching the film with a syringe needle enabled film profiling by SFM and determining the local film thicknesses above the plateaus and above the trenches for each sample (Figure 1e−g). Local film thickness values were averaged for at least four patterns on

DOI: 10.1021/acsami.9b12817
ACS Appl. Mater. Interfaces 2019, 11, 35247−35254

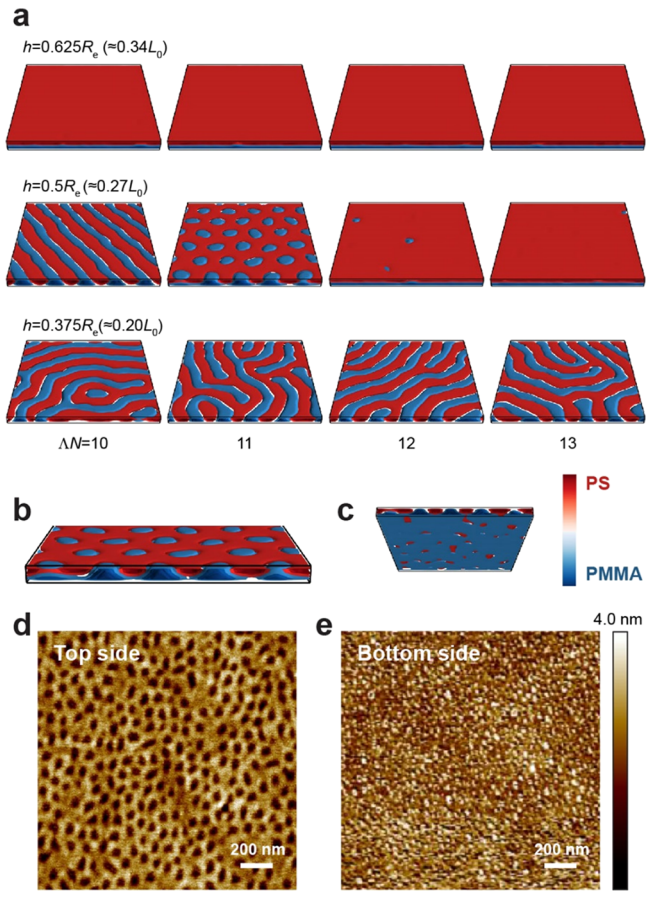

Figure 2. (a) Simulation results of the assembly of lamellar block copolymer films of different thicknesses, h, in the ultraconfined regime on selective substrates. PS and PMMA domains are depicted in red and blue, respectively; R_e and ΛN denote the average end-to-end distance of the copolymer chain and the preference of the substrate for PMMA domains, respectively. (b, c) Side and bottom views of the $h = 0.5R_e$ and $\Lambda N = 11$ system, showing (b) the neck-like cross-section of the PMMA domains and (c) the preferential substrate wetting by PMMA. (d, e) SFM images of the (d) top and (e) bottom sides of a film cast on a smooth substrate.

each sample, which differ in the lateral dimensions of the trenches and plateaus but feature the same trench depth and nominal (cast) film thickness. For each sample, the nominal film thickness, denoted as $h_{nominal}$, was measured in topographically smooth areas on the same substrate. Figure 3a shows that, in all samples, the average film thickness above the plateaus ($<h_{pl}>$) was lower than the nominal film thickness (denoted by a dashed line). Conversely, almost all average film

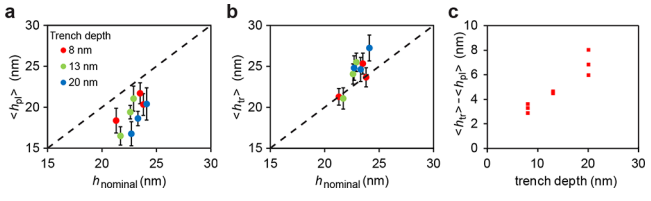

Figure 3. (a, b) Graphs showing the average film thickness above the (a) plateaus and (b) trenches compared to the nominal film thickness measured in unpatterned areas on the same sample (dashed line). (c) Dependence of the film thickness difference between the trench and plateau on the trench depth.

thicknesses above the trenches ($<h_{tr}>$) were higher than the nominal film thickness (Figure 3b). Simulations performed on a film that covers both a plateau and a trench and that take into account the difference in film thicknesses indeed reproduce the dual morphology observed experimentally (Figure 4). Additional simulations ran over 5−10 times longer show no appreciable change in morphology (Figure S4), indicating that this morphology represents a thermodynamic equilibrium.

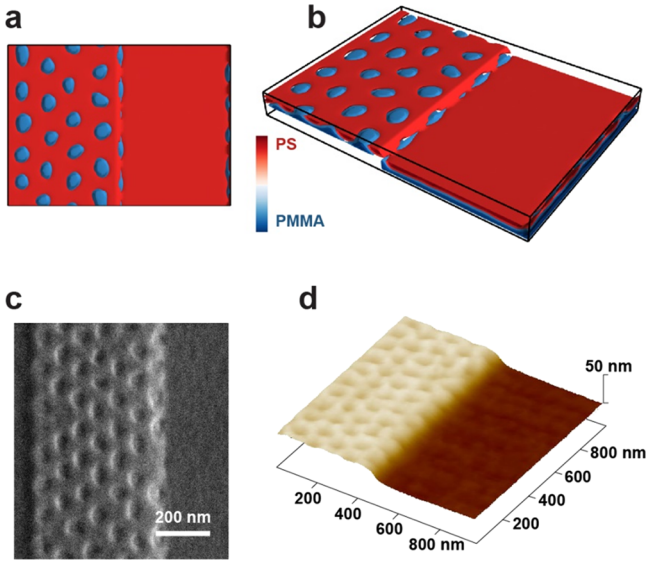

Figure 4. (a) Top view and (b) isometric view of simulation results showing the dual morphology obtained on substrates that consist of an adjacent plateau and trench. The horizontal substrate interfaces exert $\Lambda N = 11$; the sidewall of the trench exerts a slightly larger selectivity, $\Lambda N = 20$ (adjusted to match the experimental morphology). The polymer film thicknesses are $h = 0.5R_e$ and $h = 0.625R_e$ on the plateau and in the trench, respectively. (c, d) High-resolution SEM and SFM images showing the topography of the film at the edge of the plateau. The SEM image was taken at a 40° tilt.

Figure 1e−g shows that the film continues smoothly from the plateaus into the trenches. The corrugation of the top film surface does not vanish even with prolonged annealing times.[63−65] This roughness is explained by the balance of capillary forces acting on the thin polymer film. The Laplace pressure thins the film on the plateaus and increases the film thickness in the trenches. The Laplace pressure is counterbalanced by the disjoining pressure, Π[66]

$$\gamma \frac{\partial^2 h}{\partial x^2} = -\Pi(h) \quad (1)$$

where γ denotes the surface tension of the copolymer film and x denotes the lateral coordinate. The fact that the film surface is not flat indicates that the extent of the disjoining pressure is significant. This arises from the nonuniformity of the film structure in the direction normal to the substrate[67] and thus demonstrates that the experimental morphology cannot be simply standing cylinders (see additional discussion in the Supporting Information). Assuming that the surface curvature changes approximately linearly with the trench depth for a given trench width and nominal film thickness, so is the thickness difference between the trenches and plateaus, as we found experimentally (Figure 3c).

DOI: 10.1021/acsami.9b12817
ACS Appl. Mater. Interfaces 2019, 11, 35247−35254

The above discussion reveals that applying ultrathin block copolymer films on a selective substrate that is topographically defined may enable to obtain dual morphologies over different areas in a controlled fashion. The topography of the substrate could be looked upon as providing a differentiating mechanism, which causes the film in certain areas of the substrate (i.e., the trenches) to differ in thickness from other areas of the substrate (i.e., the plateaus). Then, the extreme sensitivity of morphology to film thickness leads to different patterns in each area.[42] As one of these morphologies could be lying lamellae, an important consequence is the ability to create patterned domains that are spaced by featureless domains that are defined by the topographic design, as shown in Figure 1.

The versatility of our approach for obtaining complex morphologies and patterns is further demonstrated in Figure 5.

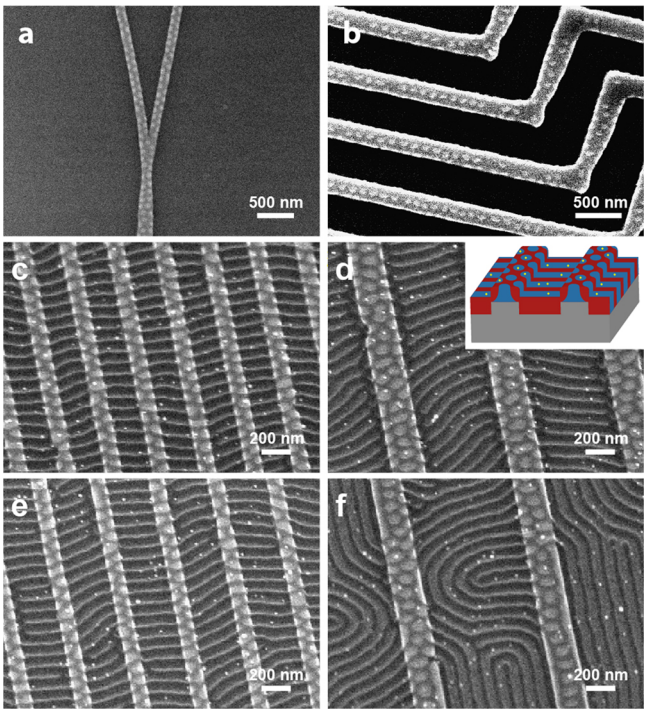

Figure 5. SEM images of: (a) a 23 nm-thick film assembled on substrates featuring 20 nm deep trenches and irregular features; (b) a 30 nm-thick film with 42 nm deep trenches in the shape of jogs; (c–f) 29 nm-thick nanocomposite films of the same PS-*b*-PMMA block copolymer co-assembled with 13 nm Au-PEO nanoparticles on patterned substrates featuring 27 nm deep trenches. Nanoparticle filling fraction in all films was 1 vol %. Trench/plateau lateral widths: (c) 160/160, (d) 480/320, (e) 240/160, and (f) 640/320 nm. The inset illustration shows the 3D morphology schematically.

First, obtaining patterned regions spaced by nonpatterned domains could be extended to plateaus featuring nonregular shapes (Figure 5a,b). Second, complex morphologies could be obtained by harnessing the ability to switch the orientation of domains with respect to the substrate from parallel to perpendicular by incorporating a small amount of nanoparticles.[54,68] Figure 5c–f shows samples with alternating dot–stripe patterns obtained by adding gold nanoparticles that were modified with thiol-terminated polyethyleneoxide ligands (M_n 5 kDa) to the BCP solution before casting. In the annealed films, these nanoparticles segregate to the PMMA domains;[69] the competition between the preference of the PMMA domains to wet the polar substrate and the tendency of the nanoparticles to segregate to the film surface to lower its surface tension causes the lamellae to orient normal to the substrate in order to expose the PMMA domains.[54] In narrow trenches, the standing lamellae are oriented across the trenches, whereas in wider trenches, they are oriented more randomly and tend to align parallel to the trench walls in some locations. This could be attributed to commensurability conditions between the nanocomposite lamellar period and the trench width. Apparently, the narrow trenches cannot accommodate complete multiples of the nanocomposite lamellae oriented along the walls, which causes its domains to orient across the trench, whereas the wider trenches can tolerate slight mismatches in commensurability. Interestingly, we note that the PMMA stripes oriented across the narrow trenches also connect the dots on different plateaus (Figure 5c–e); this may be used to induce registry between different patterned regions. Combining these conditions with a more complex design of the topographical substrate may lead to more elaborate patterns.

CONCLUSIONS

In summary, we have demonstrated that block copolymer films cast on topographically defined substrates feature different thicknesses in the plateau and trench regions. In the regime of ultraconfined films, the morphology (and hence the surface pattern) becomes very sensitive to slight variations in film thickness and substrate selectivity. Combining these two effects enables the creation of coatings showing co-existing patterns on different regions, including the ability to have patterned regions spaced arbitrarily with nonpatterned regions. Such complex patterns could be further elaborated by controlling the domain alignment and orientation, for example, by including nanoparticles.

The strength of this approach lies in its simplicity and generality. Complex patterns are easily obtained with a neat block copolymer in a single-step process. From our experience, complex patterns are also obtained with other types of block copolymers, such as polystyrene-*block*-poly(vinyl pyridine) and polystyrene-*block*-poly(lactic acid) (research in progress). It is envisioned that adding different types of fillers to different types of block copolymers could give rise to functional coatings that derive their properties from the controlled spatial arrangement of functional components. These research directions are currently underway and will be reported in due course.

EXPERIMENTAL SECTION

PS-*b*-PMMA diblock copolymer (M_n 312 kDa, PDI 1.27, 45 wt % PS, and L_0 = 84 nm) was synthesized by standard anionic polymerization under a nitrogen atmosphere. The molecular weight, size distribution, and polystyrene weight percentage were determined by gel permeation chromatography (GPC) in tetrahydrofuran against PS standards for the PS block, and comparison of the ^{1}H NMR signals for the phenyl and methoxy groups for the PMMA block. L_0 was determined by SAXS.

Gold nanoparticles were synthesized according to known procedures[70] from chloroauric acid ($HAuCl_4{\cdot}3H_2O$) and sodium citrate. The average size (13 nm) and size dispersity of the nanoparticles were determined by transmission electron microscopy (FEI Tecnai T12 G^2 Spirit TEM) and analyzed using ImageJ software. In order to affect ligand exchange,[69] the as-synthesized nanoparticles were stirred overnight at room temperature with thiol-terminated PEO ligands (M_n 5000 Da, Sigma-Aldrich). The nanoparticles were then transferred to chloroform using a small amount of ethanol as a

DOI: 10.1021/acsami.9b12817
ACS Appl. Mater. Interfaces 2019, 11, 35247–35254

co-solvent and vigorous shaking followed by washing with deionized water. The chloroform solution was concentrated by evaporation. Excess PEO-SH ligands were removed by centrifugation at 6000 rpm for 10 min with *n*-hexane as the nonsolvent. This procedure was repeated three times.

Topographically patterned substrates with varying feature sizes were prepared using electron-beam lithography (Raith e-LiNE) on silicon wafer substrates using a 250 nm-thick PMMA resist (495 kDa, Microchem) followed by cold development (2 min, −5 °C) in the MIBK:IPA (1:3) developer solution and reactive ion etching with C_4F_8 and SF_6 (Oxford Instruments Plasmalab System 100). For substrates used in nanocomposite experiments, initial patterning was done by thermal nanoimprint lithography using a 140 nm-thick PMMA resist (35 kDa, Acros) spin-coated from anisole (Sigma-Aldrich) with an in-house imprint press. Following etching, substrates were cleaned with oxygen plasma and piranha solution. Trench depths were measured using scanning force microscopy.

Block copolymer thin films were prepared on flat and patterned substrates by spin-coating toluene solutions of the BCP of various concentrations (0.4 to 1.0%, w/w) for 30 s at 3000 rpm. All films were annealed for 15 min in a closed Petri dish with a saturated chloroform vapor environment at ambient temperature. Nanocomposite films were prepared using solutions containing 250 μL of BCP in toluene (0.8 wt %) and 250 μL of Au-PEO nanoparticles in chloroform (0.021 μM, determined by UV−vis spectrometry at λ = 531 nm using ε_{531} = 2.77 × 10^8 M^{-1} cm^{-1}).[71] These solutions were spin-coated and annealed under the same conditions as described above. Some BCP films were prepared on silicon wafers featuring 100 nm-thick thermal oxide, solvent annealed, floated on a 10 vol % HF solution by slow insertion of the sample at a shallow angle, and then transferred onto HF-treated silicon wafers by touching the surface of the solution with the receiving substrate. This allowed inspecting the bottom side of these films by microscopy.

Film characterization was performed using high-resolution scanning electron microscopy (FEI Sirion HR-SEM and FEI Magellan 400 L XHR SEM) and scanning force microscopy (SFM; Dimension 3100 with Nanoscope V controller, Veeco). Film thicknesses above the trenches and plateaus were determined by scratching away part of the film with a 19 gauge syringe needle followed by SFM scanning and analysis of the seam between the intact BCP film and the exposed silicon substrate using the step analysis tool (Nanoscope Analysis Program v. 1.40, Bruker), which averages height values of different scan lines of selected areas. These thicknesses were determined by referencing to the SFM height values of the corresponding, completely exposed features. Local film thickness values were averaged for at least four patterns on each sample; error bars in Figure 3a show the corresponding standard deviation values.

Simulation Details. We use a soft, coarse-grained model to represent the copolymer melt.[72] The polymers consist of two structurally symmetric blocks (A and B), each of which is composed of $N/2$ = 32 segments. The film is confined into a volume V that is surrounded by impenetrable walls. The geometry of the confinement is adapted to the experiments (Figure S3). The top surface of the film, in contact with the chloroform vapor, is nonpreferential, whereas the substrate prefers the PMMA component via a short-range interaction of strength ΛN (see nonbonded interactions below). Although the flat substrate and the sidewalls are made of the same material (SiO_x), their values of substrate preference differ because, in the experiment, the interaction of the polymer with the substrate is composed of short-range, contact interactions and long-range, van der Waals interactions. Whereas the former are independent from the substrate geometry, the latter arise from the integration over the volume of polymer and substrate and therefore depend on substrate topography and polymer morphology. The calibration of the substrate preference by the phase behavior on a flat substrate does not allow us to distinguish between both components. Thus, we have adjusted the sidewall preference to match the experimental morphology at the boundary between plateaus and trenches.

Segments along the linear, flexible molecular backbone are connected via harmonic bonds. In the simulations, the unit of length is set by the end-to-end distance, R_e, of the polymers in the absence of confinement or nonbonded interactions. The nonbonded interactions, $\mathcal{H}_{nb}$, are composed of three parts: (i) the average repulsion between segments limits the isothermal compressibility. The corresponding coarse-grained parameter is the inverse isothermal compressibility, and, in accordance with previous studies, we use the value κN = 50. (ii) The repulsion between AB pairs is larger than that between segments of the same type such that the bare Flory−Huggins parameter is χN = 30

$$\frac{\mathcal{H}_{nb}}{\sqrt{\bar{N}}\,k_BT} = \int \frac{dr}{{R_e}^3}\left\{\frac{\kappa N}{2}[\phi_A + \phi_B - 1]^2 - \frac{\chi N}{4}[\phi_A - \phi_B]^2\right\} \quad (2)$$

where ϕ_A and ϕ_B denote the normalized densities (i.e., volume fractions) of A (PS) and B (PMMA) segments, respectively. These nonbonded interactions are evaluated via a collocation grid of linear dimension $\Delta L = R_e/8$. (iii) Additionally, there are surface fields that repel the A (PS) component and attract the B (PMMA) component with the same strength, Λ. These surface interactions extend a distance ΔL away from the substrate. The free surface of the film is nonpreferential, accounting for the similarity of the surface tensions of PS and PMMA under chloroform vapor. The average segment density, ρ_0, is set by the invariant degree of polymerization, $\sqrt{\bar{N}} \equiv \rho_0 {R_e}^3/N = 128$.

The morphologies are obtained after a quench of the system from the disordered state to χN = 30. Within self-consistent field theory, the equilibrium lamellar spacing is $L_0 \approx 1.83R_e$. The simulations employ the single-chain-in-mean-field algorithm[73] in conjunction with the Smart Monte Carlo moves that give rise to Rouse-like dynamics.[74] The simulations runs were extended to at least $T = 1.2 \times 10^6$ Monte Carlo steps (MCS), corresponding to $T = 35{R_e}^2/D$, with $D = 2.925 \times 10^{-5}$ ${R_e}^2$/MCS being the self-diffusion coefficient. Extended simulations (5−10 times longer) ran on flat and topographically patterned substrates show no appreciable change in morphology, indicating that the observed morphologies represent thermodynamic equilibria.

■ ASSOCIATED CONTENT

Supporting Information

The Supporting Information is available free of charge on the ACS Publications website at DOI: 10.1021/acsami.9b12817.

Additional SEM images (Figure S1), SFM images of thin BCP films cast at different thicknesses on flat substrates (Figure S2), illustration of the simulation cell (Figure S3), simulation results after an extended run (Figure S4), and additional discussion on the disjoining pressure and the shape of the free surface (PDF)

■ AUTHOR INFORMATION

Corresponding Authors

*E-mail: mmueller@theorie.physik.uni-goettingen.de (M.M.).
*E-mail: roys@huji.ac.il (R.S.).

ORCID

Mark Schvartzman: 0000-0002-5912-525X
Marcus Müller: 0000-0002-7472-973X
Roy Shenhar: 0000-0002-0631-1542

Author Contributions

The manuscript was written through contributions of all authors. All authors have given approval to the final version of the manuscript.

DOI: 10.1021/acsami.9b12817
ACS Appl. Mater. Interfaces 2019, 11, 35247−35254

Funding

This research was supported by the Israel Science Foundation (grant number 229/17) and the Deutsche Forschungsgemeinschaft (grant SFB 1073/TPA03).

Notes

The authors declare no competing financial interest.

■ ACKNOWLEDGMENTS

We thank Rabibrata Mukherjee for stimulating discussions. We thank Evgenia Blayvas for assistance with the XHR SEM imaging. E.M. thanks the Cambr Charitable Foundation for a Ph.D. fellowship.

■ REFERENCES

(1) Minovich, A. E.; Miroshnichenko, A. E.; Bykov, A. Y.; Murzina, T. V.; Neshev, D. N.; Kivshar, Y. S. Functional and Nonlinear Optical Metasurfaces. *Laser Photonics Rev.* **2015**, *9*, 195−213.

(2) Chen, H.-T.; Taylor, A. J.; Yu, N. A Review of Metasurfaces: Physics and Applications. *Rep. Prog. Phys.* **2016**, *79*, 076401.

(3) Xiao, S.; Yang, X.; Steiner, P.; Hsu, Y.; Lee, K.; Wago, K.; Kuo, D. Servo-Integrated Patterned Media by Hybrid Directed Self-Assembly. *ACS Nano* **2014**, *8*, 11854−11859.

(4) Ozbay, E. Plasmonics: Merging Photonics and Electronics at Nanoscale Dimensions. *Science* **2006**, *311*, 189−193.

(5) Lim, J. Y.; Donahue, H. J. Cell Sensing and Response to Micro- and Nanostructured Surfaces Produced by Chemical and Topographic Patterning. *Tissue Eng.* **2007**, *13*, 1879−1891.

(6) Schvartzman, M.; Palma, M.; Sable, J.; Abramson, J.; Hu, X.; Sheetz, M. P.; Wind, S. J. Nanolithographic Control of the Spatial Organization of Cellular Adhesion Receptors at the Single-Molecule Level. *Nano Lett.* **2011**, *11*, 1306−1312.

(7) Keydar, Y.; Le Saux, G.; Pandey, A.; Avishay, E.; Bar-Hanin, N.; Esti, T.; Bhingardive, V.; Hadad, U.; Porgador, A.; Schvartzman, M. Natural Killer Cells' Immune Response Requires a Minimal Nanoscale Distribution of Activating Antigens. *Nanoscale* **2018**, *10*, 14651−14659.

(8) Halas, N. J.; Lal, S.; Link, S.; Chang, W.-S.; Natelson, D.; Hafner, J. H.; Nordlander, P. A Plethora of Plasmonics from the Laboratory for Nanophotonics at Rice University. *Adv. Mater.* **2012**, *24*, 4842−4877.

(9) Ee, H. S.; Agarwal, R. Tunable Metasurface and Flat Optical Zoom Lens on a Stretchable Substrate. *Nano Lett.* **2016**, *16*, 2818−2823.

(10) Conway, J. A.; Sahni, S.; Szkopek, T. Plasmonic Interconnects Versus Conventional Interconnects: A Comparison of Latency, Crosstalk and Energy Costs. *Opt. Express* **2007**, *15*, 4474−4484.

(11) Rockford, L.; Liu, Y.; Mansky, P.; Russell, T. P.; Yoon, M.; Mochrie, S. G. J. Polymers on Nanoperiodic, Heterogeneous Surfaces. *Phys. Rev. Lett.* **1999**, *82*, 2602−2605.

(12) Kim, S. O.; Solak, H. H.; Stoykovich, M. P.; Ferrier, N. J.; de Pablo, J. J.; Nealey, P. F. Epitaxial Self-Assembly of Block Copolymers on Lithographically Defined Nanopatterned Substrates. *Nature* **2003**, *424*, 411−414.

(13) Cheng, J. Y.; Mayes, A. M.; Ross, C. A. Nanostructure Engineering by Templated Self-Assembly of Block Copolymers. *Nat. Mater.* **2004**, *3*, 823−828.

(14) Ruiz, R.; Kang, H.; Detcheverry, F. A.; Dobisz, E.; Kercher, D. S.; Albrecht, T. R.; de Pablo, J. J.; Nealey, P. F. Density Multiplication and Improved Lithography by Directed Block Copolymer Assembly. *Science* **2008**, *321*, 936−939.

(15) Sundrani, D.; Darling, S. B.; Sibener, S. J. Guiding Polymers to Perfection: Macroscopic Alignment of Nanoscale Domains. *Nano Lett.* **2004**, *4*, 273−276.

(16) Segalman, R. A.; Yokoyama, H.; Kramer, E. J. Graphoepitaxy of Spherical Domain Block Copolymer Films. *Adv. Mater.* **2001**, *13*, 1152−1155.

(17) Borah, D.; Shaw, M. T.; Holmes, J. D.; Morris, M. A. Sub-10 Nm Feature Size Ps-B-Pdms Block Copolymer Structures Fabricated by a Microwave-Assisted Solvothermal Process. *ACS Appl. Mater. Interfaces* **2013**, *5*, 2004−2012.

(18) Han, E.; Kang, H.; Liu, C.-C.; Nealey, P. F.; Gopalan, P. Graphoepitaxial Assembly of Symmetric Block Copolymers on Weakly Preferential Substrates. *Adv. Mater.* **2010**, *22*, 4325−4329.

(19) Tavakkoli K G, A.; Nicaise, S. M.; Gadelrab, K. R.; Alexander-Katz, A.; Ross, C. A.; Berggren, K. K. Multilayer Block Copolymer Meshes by Orthogonal Self-Assembly. *Nat. Commun.* **2016**, *7*, 10518.

(20) Majewski, P. W.; Rahman, A.; Black, C. T.; Yager, K. G. Arbitrary Lattice Symmetries Via Block Copolymer Nanomeshes. *Nat. Commun.* **2015**, *6*, 7448.

(21) Tavakkoli K G, A.; Gotrik, K. W.; Hannon, A. F.; Alexander-Katz, A.; Ross, C. A.; Berggren, K. K. Templating Three-Dimensional Self-Assembled Structures in Bilayer Block Copolymer Films. *Science* **2012**, *336*, 1294−1298.

(22) Cha, S. K.; Yong, D.; Yang, G. G.; Jin, H. M.; Kim, J. H.; Han, K. H.; Kim, J. U.; Jeong, S.-J.; Kim, S. O. Nanopatterns with a Square Symmetry from an Orthogonal Lamellar Assembly of Block Copolymers. *ACS Appl. Mater. Interfaces* **2019**, *11*, 20265−20271.

(23) Rahman, A.; Majewski, P. W.; Doerk, G.; Black, C. T.; Yager, K. G. Non-Native Three-Dimensional Block Copolymer Morphologies. *Nat. Commun.* **2016**, *7*, 13988.

(24) Jin, C.; Olsen, B. C.; Wu, N. L. Y.; Luber, E. J.; Buriak, J. M. Sequential Nanopatterned Block Copolymer Self-Assembly on Surfaces. *Langmuir* **2016**, *32*, 5890−5898.

(25) Jin, C.; Olsen, B. C.; Luber, E. J.; Buriak, J. M. Preferential Alignment of Incommensurate Block Copolymer Dot Arrays Forming Moiré Superstructures. *ACS Nano* **2017**, *11*, 3237−3246.

(26) Lee, S.; Cheng, L. C.; Gadelrab, K. R.; Ntetsikas, K.; Moschovas, D.; Yager, K. G.; Avgeropoulos, A.; Alexander-Katz, A.; Ross, C. A. Double-Layer Morphologies from a Silicon-Containing ABA Triblock Copolymer. *ACS Nano* **2018**, *12*, 6193−6202.

(27) Chai, J.; Buriak, J. M. Using Cylindrical Domains of Block Copolymers to Self-Assemble and Align Metallic Nanowires. *ACS Nano* **2008**, *2*, 489−501.

(28) Stoykovich, M. P.; Müller, M.; Kim, S. O.; Solak, H. H.; Edwards, E. W.; de Pablo, J. J.; Nealey, P. F. Directed Assembly of Block Copolymer Blends into Nonregular Device-Oriented Structures. *Science* **2005**, *308*, 1442−1446.

(29) Stoykovich, M. P.; Kang, H.; Daoulas, K. C.; Liu, G.; Liu, C. C.; de Pablo, J. J.; Müller, M.; Nealey, P. F. Directed Self-Assembly of Block Copolymers for Nanolithography: Fabrication of Isolated Features and Essential Integrated Circuit Geometries. *ACS Nano* **2007**, *1*, 168−175.

(30) Liu, G.; Thomas, C. S.; Craig, G. S. W.; Nealey, P. F. Integration of Density Multiplication in the Formation of Device-Oriented Structures by Directed Assembly of Block Copolymer-Homopolymer Blends. *Adv. Funct. Mater.* **2010**, *20*, 1251−1257.

(31) Yang, J. K. W.; Jung, Y. S.; Chang, J. B.; Mickiewicz, R. A.; Alexander-Katz, A.; Ross, C. A.; Berggren, K. K. Complex Self-Assembled Patterns Using Sparse Commensurate Templates with Locally Varying Motifs. *Nat. Nanotechnol.* **2010**, *5*, 256−260.

(32) Chang, J.-B.; Choi, H. K.; Hannon, A. F.; Alexander-Katz, A.; Ross, C. A.; Berggren, K. K. Design Rules for Self-Assembled Block Copolymer Patterns Using Tiled Templates. *Nat. Commun.* **2014**, *5*, 3305.

(33) Tavakkoli K G, A.; Nicaise, S. M.; Hannon, A. F.; Gotrik, K. W.; Alexander-Katz, A.; Ross, C. A.; Berggren, K. K. Sacrificial-Post Templating Method for Block Copolymer Self-Assembly. *Small* **2014**, *10*, 493−499.

(34) Herr, D. J. C. Directed Block Copolymer Self-Assembly for Nanoelectronics Fabrication. *J. Mater. Res.* **2011**, *26*, 122−139.

(35) Do, H. W.; Choi, H. K.; Gadelrab, K. R.; Chang, J. B.; Alexander-Katz, A.; Ross, C. A.; Berggren, K. K. Directed Self-Assembly of a Two-State Block Copolymer System. *Nano Convergence* **2018**, *5*, 25.

DOI: 10.1021/acsami.9b12817
ACS Appl. Mater. Interfaces 2019, 11, 35247−35254

(36) Chang, T.-H.; Xiong, S.; Liu, C.-C.; Liu, D.; Nealey, P. F.; Ma, Z. The One-Pot Directed Assembly of Cylinder-Forming Block Copolymer on Adjacent Chemical Patterns for Bimodal Patterning. *Macromol. Rapid Commun.* **2017**, *38*, 1700285.
(37) Stein, A.; Wright, G.; Yager, K. G.; Doerk, G. S.; Black, C. T. Selective Directed Self-Assembly of Coexisting Morphologies Using Block Copolymer Blends. *Nat. Commun.* **2016**, *7*, 12366.
(38) Son, J. G.; Chang, J. B.; Berggren, K. K.; Ross, C. A. Assembly of Sub-10-Nm Block Copolymer Patterns with Mixed Morphology and Period Using Electron Irradiation and Solvent Annealing. *Nano Lett.* **2011**, *11*, 5079−5084.
(39) Qiang, Z.; Akolawala, S. A.; Wang, M. Simultaneous in-Film Polymer Synthesis and Self-Assembly for Hierarchical Nanopatterns. *ACS Macro Lett.* **2018**, *7*, 566−571.
(40) Jeong, S. J.; Moon, H. S.; Kim, B. H.; Kim, J. Y.; Yu, J.; Lee, S.; Lee, M. G.; Choi, H.; Kim, S. O. Ultralarge-Area Block Copolymer Lithography Enabled by Disposable Photoresist Prepatterning. *ACS Nano* **2010**, *4*, 5181−5186.
(41) Zhao, W.; Li, W. Hybrid patterns from directed self-assembly of diblock copolymers by chemical patterns. *Phys. Chem. Chem. Phys.* **2019**, *21*, 18525−18532.
(42) Zhao, W.; Duan, C.; Li, W. Hybrid line−dot nanopatterns from directed self-assembly of diblock copolymers by trenches. *Phys. Chem. Chem. Phys.* **2019**, *21*, 10011−10021.
(43) Bita, I.; Yang, J. K. W.; Jung, Y. S.; Ross, C. A.; Thomas, E. L.; Berggren, K. K. Graphoepitaxy of Self-Assembled Block Copolymers on Two-Dimensional Periodic Patterned Templates. *Science* **2008**, *321*, 939−943.
(44) Cheng, J. Y.; Ross, C. A.; Thomas, E. L.; Smith, H. I.; Vancso, G. J. Fabrication of Nanostructures with Long-Range Order Using Block Copolymer Lithography. *Appl. Phys. Lett.* **2002**, *81*, 3657−3659.
(45) Choi, J.; Li, Y.; Kim, P. Y.; Liu, F.; Kim, H.; Yu, D. M.; Huh, J.; Carter, K. R.; Russell, T. P. Orthogonally Aligned Block Copolymer Line Patterns on Minimal Topographic Patterns. *ACS Appl. Mater. Interfaces* **2018**, *10*, 8324−8332.
(46) Yang, X.; Xiao, S.; Hu, W.; Hwu, J.; van de Veerdonk, R.; Wago, K.; Lee, K.; Kuo, D. Integration of Nanoimprint Lithography with Block Copolymer Directed Self-Assembly for Fabrication of a Sub-20 Nm Template for Bit-Patterned Media. *Nanotechnology* **2014**, *25*, 395301.
(47) Li, H. W.; Huck, W. T. S. Ordered Block-Copolymer Assembly Using Nanoimprint Lithography. *Nano Lett.* **2004**, *4*, 1633−1636.
(48) Doerk, G. S.; Cheng, J. Y.; Singh, G.; Rettner, C. T.; Pitera, J. W.; Balakrishnan, S.; Arellano, N.; Sanders, D. P. Enabling Complex Nanoscale Pattern Customization Using Directed Self-Assembly. *Nat. Commun.* **2014**, *5*, 5805.
(49) Kim, E.; Ahn, H.; Park, S.; Lee, H.; Lee, M.; Lee, S.; Kim, T.; Kwak, E.-A.; Lee, J. H.; Lei, X.; Huh, J.; Bang, J.; Lee, B.; Ryu, D. Y. Directed Assembly of High Molecular Weight Block Copolymers: Highly Ordered Line Patterns of Perpendicularly Oriented Lamellae with Large Periods. *ACS Nano* **2013**, *7*, 1952−1960.
(50) Choi, E.; Park, S.; Ahn, H.; Lee, M.; Bang, J.; Lee, B.; Ryu, D. Y. Substrate-Independent Lamellar Orientation in High-Molecular-Weight Polystyrene-B-Poly(Methyl Methacrylate) Films: Neutral Solvent Vapor and Thermal Annealing Effect. *Macromolecules* **2014**, *47*, 3969−3977.
(51) Chen, F.; Akasaka, S.; Inoue, T.; Takenaka, M.; Hasegawa, H.; Yoshida, H. Ordering Cylindrical Microdomains for Binary Blends of Block Copolymers with Graphoepitaxy. *Macromol. Rapid Commun.* **2007**, *28*, 2137−2144.
(52) Stuen, K. O.; Detcheverry, F. A.; Craig, G. S. W.; Thomas, C. S.; Farrell, R. A.; Morris, M. A.; de Pablo, J. J.; Nealey, P. F. Graphoepitaxial Assembly of Asymmetric Ternary Blends of Block Copolymers and Homopolymers. *Nanotechnology* **2010**, *21*, 495301.
(53) Aprile, G.; Ferrarese Lupi, F.; Fretto, M.; Enrico, E.; De Leo, N.; Boarino, L.; Volpe, F. G.; Seguini, G.; Sparnacci, K.; Gianotti, V.; Laus, M.; Garnæs, J.; Perego, M. Toward Lateral Length Standards at the Nanoscale Based on Diblock Copolymers. *ACS Appl. Mater. Interfaces* **2017**, *9*, 15685−15697.
(54) Halevi, A.; Halivni, S.; Oded, M.; Müller, A. H. E.; Banin, U.; Shenhar, R. Co-Assembly of a-B Diblock Copolymers with B'-Type Nanoparticles in Thin Films: Effect of Copolymer Composition and Nanoparticle Shape. *Macromolecules* **2014**, *47*, 3022−3032.
(55) Morkved, T. L.; Jaeger, H. M. Thickness-Induced Morphology Changes in Lamellar Diblock Copolymer Ultrathin Films. *Europhys. Lett.* **1997**, *40*, 643−648.
(56) Fasolka, M. J.; Mayes, A. M. Block Copolymer Thin Films: Physics and Applications. *Annu. Rev. Mater. Res.* **2001**, *31*, 323−355.
(57) Li, W.; Liu, M.; Qiu, F.; Shi, A.-C. Phase Diagram of Diblock Copolymers Confined in Thin Films. *J. Phys. Chem. B* **2013**, *117*, 5280−5288.
(58) Knoll, A.; Horvat, A.; Lyakhova, K. S.; Krausch, G.; Sevink, G. J. A.; Zvelindovsky, A. V.; Magerle, R. Phase Behavior in Thin Films of Cylinder-Forming Block Copolymers. *Phys. Rev. Lett.* **2002**, *89*, 035501.
(59) Horvat, A.; Lyakhova, K. S.; Sevink, G. J. A.; Zvelindovsky, A. V.; Magerle, R. Phase Behavior in Thin Films of Cylinder-Forming ABA Block Copolymers: Mesoscale Modeling. *J. Chem. Phys.* **2004**, *120*, 1117−1126.
(60) Xuan, Y.; Peng, J.; Cui, L.; Wang, H.; Li, B.; Han, Y. Morphology Development of Ultrathin Symmetric Diblock Copolymer Film Via Solvent Vapor Treatment. *Macromolecules* **2004**, *37*, 7301−7307.
(61) Park, S.; Tsarkova, L.; Hiltl, S.; Roitsch, S.; Mayer, J.; Böker, A. Guiding Block Copolymers into Sequenced Patterns Via Inverted Terrace Formation. *Macromolecules* **2012**, *45*, 2494−2501.
(62) Park, S.; Tsarkova, L. A. Surface Roughness-Mediated Ordering in Block Copolymer Films toward Spatially Controlled Patterns. *Macromolecules* **2017**, *50*, 6840−6848.
(63) Li, Z.; Tolan, M.; Höhr, T.; Kharas, D.; Qu, S.; Sokolov, J.; Rafailovich, M. H.; Lorenz, H.; Kotthaus, J. P.; Wang, J.; Sinha, S. K.; Gibaud, A. Polymer Thin Films on Patterned Si Surfaces. *Macromolecules* **1998**, *31*, 1915−1920.
(64) Rehse, N.; Wang, C.; Hund, M.; Geoghegan, M.; Magerle, R.; Krausch, G. Stability of Thin Polymer Films on a Corrugated Substrate. *Eur. Phys. J. E: Soft Matter Biol. Phys.* **2001**, *4*, 69−76.
(65) Roy, S.; Ansari, K. J.; Jampa, S. S. K.; Vutukuri, P.; Mukherjee, R. Influence of Substrate Wettability on the Morphology of Thin Polymer Films Spin-Coated on Topographically Patterned Substrates. *ACS Appl. Mater. Interfaces* **2012**, *4*, 1887−1896.
(66) Indekeu, J. O. Line Tension near the Wetting Transition - Results from an Interface Displacement Model. *Phys. A* **1992**, *183*, 439−461.
(67) Man, X.; Andelman, D.; Orland, H. Block Copolymer Films with Free Interfaces: Ordering by Nanopatterned Substrates. *Phys. Rev. E* **2012**, *86*, 010801.
(68) Lin, Y.; Böker, A.; He, J.; Sill, K.; Xiang, H.; Abetz, C.; Li, X.; Wang, J.; Emrick, T.; Long, S.; Wang, Q.; Balazs, A.; Russell, T. P. Self-Directed Self-Assembly of Nanoparticle/Copolymer Mixtures. *Nature* **2005**, *434*, 55−59.
(69) Ploshnik, E.; Langner, K. M.; Halevi, A.; Ben-Lulu, M.; Müller, A. H. E.; Fraaije, J. G. E. M.; Agur Sevink, G. J.; Shenhar, R. Hierarchical Structuring in Block Copolymer Nanocomposites through Two Phase-Separation Processes Operating on Different Time Scales. *Adv. Funct. Mater.* **2013**, *23*, 4215−4226.
(70) Grabar, K. C.; Freeman, R. G.; Hommer, M. B.; Natan, M. J. Preparation and Characterization of Au Colloid Monolayers. *Anal. Chem.* **1995**, *67*, 735−743.
(71) Liu, X.; Atwater, M.; Wang, J.; Huo, Q. Extinction Coefficient of Gold Nanoparticles with Different Sizes and Different Capping Ligands. *Colloids Surf., B* **2007**, *58*, 3−7.
(72) Müller, M. Studying Amphiphilic Self-Assembly with Soft Coarse-Grained Models. *J. Stat. Phys.* **2011**, *145*, 967−1016.
(73) Daoulas, K. C.; Müller, M. Single Chain in Mean Field Simulations: Quasi-Instantaneous Field Approximation and Quantitative Comparison with Monte Carlo Simulations. *J. Chem. Phys.* **2006**, *125*, 184904.

DOI: 10.1021/acsami.9b12817
ACS Appl. Mater. Interfaces 2019, 11, 35247−35254

(74) Müller, M.; Daoulas, K. C. Single-Chain Dynamics in a Homogeneous Melt and a Lamellar Microphase: A Comparison between Smart Monte Carlo Dynamics, Slithering-Snake Dynamics, and Slip-Link Dynamics. *J. Chem. Phys.* **2008**, *129*, 164906.

DOI: 10.1021/acsami.9b12817
ACS Appl. Mater. Interfaces 2019, 11, 35247−35254